Peer-reviewed version available at *Biomolecules* **2018**, *8*, 90; doi:10.3390/biom8030090

Article

Numerical simulation and FRAP experiments show that the plasma membrane binding protein PH-EFA6 does not exhibit anomalous sub-diffusion in cells.

Cyril Favard [1,*]

[1] Membrane Domains and Viral Assembly, IRIM, UMR 9004 CNRS - Université Montpellier, 1919, route de Mende, 34 000 Montpellier, France; cyril.favard@irim.cnrs.fr

* Correspondence: cyril.favard@irim.cnrs.fr

Abstract: FRAP technique have been used for decades to measure movements of molecules in 2D. Data obtained by FRAP experiments in cell plasma membranes are assumed to be described through means of two parameters, a diffusion coefficient D (as defined in a pure Brownian model) and a mobile fraction M. Nevertheless, it has also been shown that recoveries can be nicely fit using anomalous sub-diffusion. FRAP at variable radii has been developed using the Brownian diffusion model to access geometrical characteristics of the surrounding landscape of the molecule. Here we performed numerical simulations of continuous time random walk (CTRW) anomalous subdiffusion and interpreted them in the context of variable radii FRAP. These simulations were compared to experimental data obtained at variable radii on living cells using the PH domain of the membrane binding protein EFA6 (exchange factor for ARF6, a small G protein). This protein domain is an excellent candidate to explore the structure of the interface between cytosol and plasma membrane in cells. By direct comparison of our numerical simulations to the experiments, we show that this protein does not exhibit anomalous diffusion in BHK cells. The non Brownian PH-EFA6 dynamics observed here is more related to spatial heterogeneities such as cytoskeleton fences effects.

Keywords: Anomalous diffusion; FRAP; Numerical Simulations; PH - Domain, Membrane Binding

1. Introduction

Early models of the plasma membrane, notably the fluid mosaic model [1] postulated that transmembrane proteins were freely diffusing in a sea of lipids. During these two last decades, it has become apparent that cell surface membranes are far from being homogeneous mixture of their lipid and protein components. They are compartmented into domains whose composition, physical properties and function are different. Numerous studies on transmembrane proteins and plasma membrane lipids by means of single particle tracking (SPT), Fluorescence Correlation Spectroscopy (FCS) or fluorescence recovery after photobleaching (FRAP) has shown the existence of micrometer and nanometer size domains on both model membrane [2,3] and living cells[4–6]. In the plasma membrane of living cells, these domains can come from different origins, but are generally classified into two main groups :

- "rafts" model where lipid/lipid phase separation drives the lateral partitioning of transmembrane proteins. [7]
- "cytoskeleton fence" model in which transmembrane proteins are coralled by a fence of cytoskeleton just beneath the plasma membrane. [8,9]

Preprints (www.preprints.org) | NOT PEER-REVIEWED | Posted: 19 July 2018 doi:10.20944/preprints201807.0356.v1

Peer-reviewed version available at Biomolecules 2018, 8, 90; doi:10.3390/biom8030090

Variable radii FRAP first [5,6], then spot variation FCS [10–12] helped in discriminate amongst these two models the nature of the deviation to pure Brownian diffusion of membrane components in living cells.

FRAP experiments have been used for determination of long-range molecular diffusion of proteins and lipids on both model system and cells for more than 30 years [13,14]. Briefly, fluorescently labelled molecules localized within a predefined area are irreversibly photo-destructed by a short and intense laser pulse. The recovery of the fluorescence in this area is then measured against time. Since no reversible photoreaction occurs, recovery of the fluorescence in the photobleached area is due to diffusion. FRAP data are generally interpreted by assuming classical Brownian diffusion. Two parameters can then be obtained : D, the lateral diffusion coefficient and M, the mobile fraction of the diffusing molecule. When the radius of the photobleached area is small compared to the diffusion area, M must be equal to 1 for freely diffusing species. In fact, most of the data reported so far in biological membranes for transmembrane proteins shows a value of $M < 1$. This lack in total fluorescence recovery can be interpreted as a restriction to free-diffusion behaviour. Parameters obtained have then to be re-evaluated to recognize the effect of time-dependent interactions in a field of random energy barriers.

An experimental approach to that question has been proposed by Feder *et al.* [15] by introducing anomalous (sub)diffusion in the motion of transmembrane proteins. Many sources of motion restriction can lead to anomalous diffusion (for review see [16] and [17]. Saxton has performed extensive numerical simulations to help in identifying the sources of anomalous diffusion (obstacles, binding...) using SPT measurements [18,19] and he declined this more recently to FRAP experiments [20] using fractional Brownian motion (fBm) or continuous time random walk (CTRW) models as sources of anomalous diffusion.

Membrane bound proteins should also be submitted to several interactions with their surrounding environment that should account for an anomalous subdiffusion behaviour. Sources of deviation from Brownian motion in their lateral diffusion may include lipid domains trapping, binding to immobile proteins and/or obstruction by cytoskeletal elements. This different possible interactions can exhibit different characteristic times, or different distributions of characteristic times. Here, diffusion of an intracellular membrane-bound protein domain (pleckstrin homology domain of EFA6, the ARF6 exchange factor) has been analysed inside living cells by FRAP experiments. Previous studies have shown that these proteins are linked to the polar head of $PI(4,5)P_2$ lipids by means of electrostatic interactions[21]. Furthermore, the protein used in this study appears to have a functional requirement to be associated to the plasma membrane within cells [22,23]

In this paper, numerical simulation of the CTRW model of anomalous sub-diffusion were first performed at a single spot size. Based on the quality of the fit using different analytical expression, we tested the ability to retrieve this anomalous diffusion in the simulated recovery curves first and in the experimental one afterwards. We showed that performing FRAP experiments at a single spot size did not allow to discriminate between the CTRW induced anomalous diffusion case and the empirical classical approach using mobile and immobile fraction.

We then computed and performed experimental FRAP at variable radii. By plotting changes in the anomality of the diffusion or in the mobile fraction as a function of the inverse of the bleached radius, as in Salomé *et al.* [5] we showed that it was possible to discriminate between the two models. Interestingly we observed that the restriction to the mobility of the PH-EFA6 domain is not due to CTRW anomalous sub diffusion, but more certainly to the sub cortical actin fences.

Preprints (www.preprints.org) | NOT PEER-REVIEWED | Posted: 19 July 2018 doi:10.20944/preprints201807.0356.v1

Peer-reviewed version available at Biomolecules 2018, 8, 90; doi:10.3390/biom8030090

2. Results

2.1. Anomalous sub-diffusion Modeling

A way to describe the continuous time random walk sub-diffusion is to start from a two dimensional random diffusion process. A particle walks from trap to trap and spend a certain (random) time in each trap. It is characterized by the following operation :

$$\mathbf{r} \rightarrow \mathbf{r} + \mathbf{\Delta}; t \rightarrow t + \tau \tag{1}$$

$\mathbf{r}$ and t are respectively the two dimensional position and the age of the particle, where $\mathbf{\Delta}$ is a two dimensional random (Gaussian) variable with variance $v = 2D$, and τ is the (random) time the particle spend into the trap.

In our model, the particle is supposed to diffuse very rapidly between two traps. This travel time is therefore neglected (this, because it was not experimentally accessible). The time τ the particle stays in a trap is supposed to have very strong fluctuations, this give rise to anomalous diffusion pattern.

As an example a generic distribution is used which leads, after a while, to a standard Levy law in time :

$$P_0(\tau) = \frac{\alpha}{(1+\tau)^{\alpha+1}} \tag{2}$$

This distribution have been used in the same type of context by Naggle [24].

The Levy exponent α is the characteristic exponent of subdiffusive behaviour. For long times we have :

$$< r^2(t) > \propto t^{\alpha} \tag{3}$$

When $\alpha < 1$ a spatio-temporal Fourier (Laplace) analysis leads to the following asymptotic (ω, $k \rightarrow 0$) Green function :

$$\tilde{g}(\mathbf{k}, \omega) \;=\; \frac{1}{\omega(D_\alpha k^2 \omega^{-\alpha} + 1)} \; ; D_\alpha = D/\Gamma(1-\alpha) \tag{4}$$

where ω and $\mathbf{k}$ are respectively the conjugate variables of position $\mathbf{r}$ and time t, where $k = |\mathbf{k}|$. Notice that the solution of the inverse Laplace transform is a function of the variable $k^2 t^{\alpha}$. It follows that the Green function is a function of the variable $x = r^2/t^{\alpha}$. When x is high enough one can perform an approximate inverse transformation via a saddle point method :

$$g(\mathbf{r}, t) \;\propto\; \exp(-cst\; x^{\nu}) \;\; ; \; \nu = \frac{1}{2-\alpha}, \; cst: \text{ a known constant} \tag{5}$$

Notice that the exponent ν interpolate nicely between the gaussian case ($\alpha = 1$) and the exponential case. The general solution of this type of anomalous diffusion process is then :

$$\rho(\mathbf{r}, t) = \int \rho_0(\mathbf{r}' - \mathbf{r}) g(x(r', t))\; d^2\mathbf{r}' \tag{6}$$

where ρ is the probability density to find the particle at the point $\mathbf{r}$ at instant t and ρ_0 is the initial state.

As the Green function is a bell-shaped fast decreasing function, one approximate it by a Gaussian shape with the exact dispersion, $D_\alpha = D \sin(\pi\alpha)/(\pi\alpha)$, which can be calculated from eq.4. This permits to construct an analytical expression of the fluorescence recovery using standard properties of Gaussian functions.

Starting from Axelrod [13] initial density as it is immediately after a Gaussian laser beam profile extinction indeed :

$$\rho_0(\mathbf{r}) = \exp(-K \exp(-2\frac{\mathbf{r}^2}{R^2})) \tag{7}$$

Preprints (www.preprints.org) | NOT PEER-REVIEWED | Posted: 19 July 2018 doi:10.20944/preprints201807.0356.v1

Peer-reviewed version available at Biomolecules 2018, 8, 90; doi:10.3390/biom8030090

(K=photobleaching constant, depending on experimental conditions [13]) and using the standard properties of the Gaussian shape in the convolution operation, one can obtain the time evolved result as a series.

Once integrated upon a disk of radius R, and, after normalization to the surface of the disk, one obtain the FRAP signal :

$$I_R(t) \;=\; 1 + \sum_{1}^{\infty} \frac{(-K)^n}{n!} \frac{1}{2n} \left(1 - \exp\left(-\frac{2nR^2}{R^2 + 4nD_\alpha t^\alpha}\right)\right) \tag{8}$$

This function will be used to fit experimental data.

Systematic corrections of this procedure are determined using numerical Monte-Carlo simulations of the fluorescence recoveries, using known α and $D = D_\alpha \frac{(\pi\alpha)}{\sin(\pi\alpha)}$

In order to keep in our calculation the finite size effects, the simulation were made in a ring of a radius of 30 arbitrary unit (a.u.) length explored by 10^7 particles for each recovery. Radii varying from 0.5 to 3 a.u. were photo-destructed during the simulation. Reflective type of boundary conditions were used. This means that when a particle gets out of the 30 a.u. radius it is re-introduced in the same direction at a small distance of the boundary. See Appendix A for examples of recovery curves generated numerically by this approach.

2.2. Validating numerical simulation and analytical models

In order to verify the validity of our analytical model, a set of numerically simulated recovery curves using anomalous diffusion as a model has been fitted with equation 8. Each parameter (α and D) were tested. Figure 1a shows the value of D obtained after fit of the numerical (D_{output}) simulation using given D (D_{input}) for the three different α tested above. Figure 1b illustrates the variation of fitted α as a function of D used in the simulation, for α =0.6 (red); α =0.7 (green); α =0.8 (blue). This clearly shows that both parameters (α,D) are always underestimated when fitting with an analytical model the numerically simulated fluorescence recoveries.

Preprints (www.preprints.org) | NOT PEER-REVIEWED | Posted: 19 July 2018 doi:10.20944/preprints201807.0356.v1

Peer-reviewed version available at Biomolecules 2018, 8, 90; doi:10.3390/biom8030090

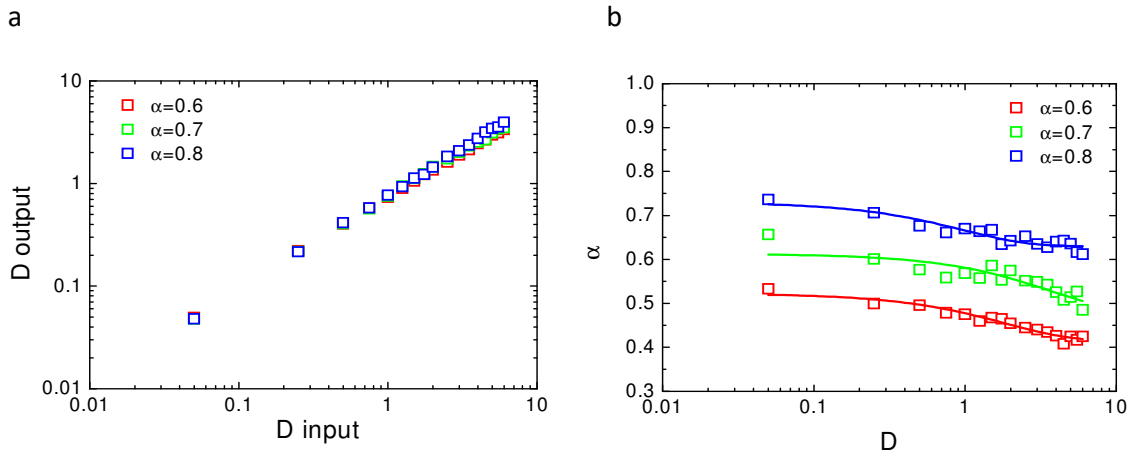

Figure 1. Values of the parameters (D, α) obtained from the fit of the simulated recoveries a- D values obtained after fit of the fluorescence recovery with eq.8 (D_{output}) as a function of D values used in the numerical simulation (D_{input}) for different α. Note that the slope is always less than 1 b- Values of α obtained after fit of the simulated curves with eq. 8 for different α used in the simulation and as a function of the D values used in the simulation. Note that the original α value used in the simulation is never reached by fit of the simulated recoveries.

This is mainly due to the finite size and finite time effect of our numerical simulations and paradoxically is also nicely mimicking what could occur experimentally in a finite size cell reservoir.

2.3. Challenging analytical models to identify numerically simulated anomalous diffusion fluorescence recoveries

Fluorescence recoveries have been numerically simulated using CTRW anomalous diffusion as the model of molecular motion. These curves were then fitted with three different analytical expression of FRAP recoveries, each being specific of a diffusion model :

- Anomalous diffusion motion (aDm): see eq. 8 in section 2.1
- Free Brownian motion (Bm) :

$$I_R(t) = \sum_1^{\infty} \frac{(-K)^n}{n!} \frac{1}{1 + n + \frac{8nDt}{R^2}} \tag{9}$$

- Restricted Brownian motion (rBm) :

$$I_R(t) = (1 - M)\frac{1 - e^{-K}}{K} + M \sum_1^{\infty} \frac{(-K)^n}{n!} \frac{1}{1 + n + \frac{8nDt}{R^2}} \tag{10}$$

where M accounts for the mobile fraction.

Preprints (www.preprints.org) | NOT PEER-REVIEWED | Posted: 19 July 2018 doi:10.20944/preprints201807.0356.v1

Peer-reviewed version available at Biomolecules 2018, 8, 90; doi:10.3390/biom8030090

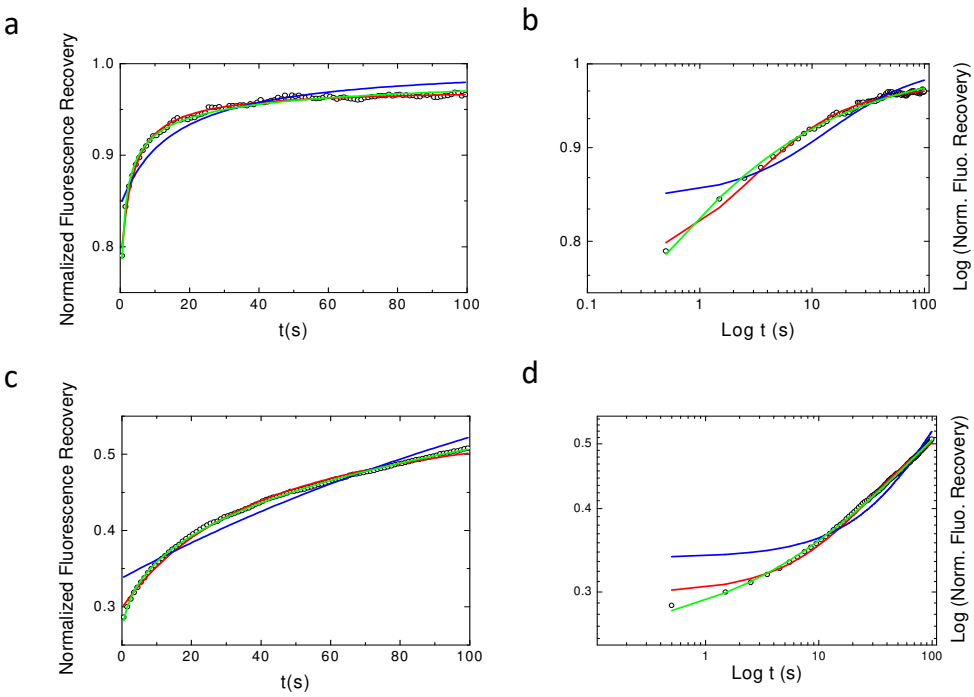

Figure 2. Best fits using the different models of Normal and Log-Log plots of simulated CTRW anomalous sub-diffusion recoveries. $\alpha = 0.6$ is the value used for the simulation in the four plots. In blue, Bm model (eq. 9), in red rBM model (eq.10) and in green aDm (eq.8) fits. In **a & b** D=2 and in **c & d** D=0.1. **a & c** are the normal plots while **b & d** are the log-log plots. From these graph it can be seen that one can hardly distinguish between the rBm model (red) and the aDm model (green) fits of the simulated recovery.

Figure 2 shows the obtained results for the three tested models (aDm in green, fBm in blue, rBm in red) with two different values of D_α and with α=0.6. It can easily be seen that the fBm does not fit to the curve, as expected, but surprisingly it can also be seen that aDm and RBm models fit quasi equivalently the numerical simulation. Even log-log plot (Fig. 2 b and d) hardly allows to directly separate the two-models. Still log-log plots show that these models can be discriminated at short times ($t \ll \tau_c$,τ_c being the characteristic half-time of the recovery) and at very long times($t \gg \tau_c$).

2.4. Single spot FRAP does not allow to identify the nature of PH-EFA6 diffusion in cells.

FRAP experiments have been performed on 15 different BHK cells (3 recoveries per cells on average) expressing the PH domain of EFA6 linked to the GFP. These data have been acquired at a given radius using the 63x objective (see experimental section for explanation). EFA 6, an exchange factor for ARF 6 (a small G protein) has recently been described as being located on the internal part of the plasma membrane, with its PH domain responsible for the interaction with lipids [23].

Preprints (www.preprints.org) | NOT PEER-REVIEWED | Posted: 19 July 2018 doi:10.20944/preprints201807.0356.v1

Peer-reviewed version available at Biomolecules 2018, 8, 90; doi:10.3390/biom8030090

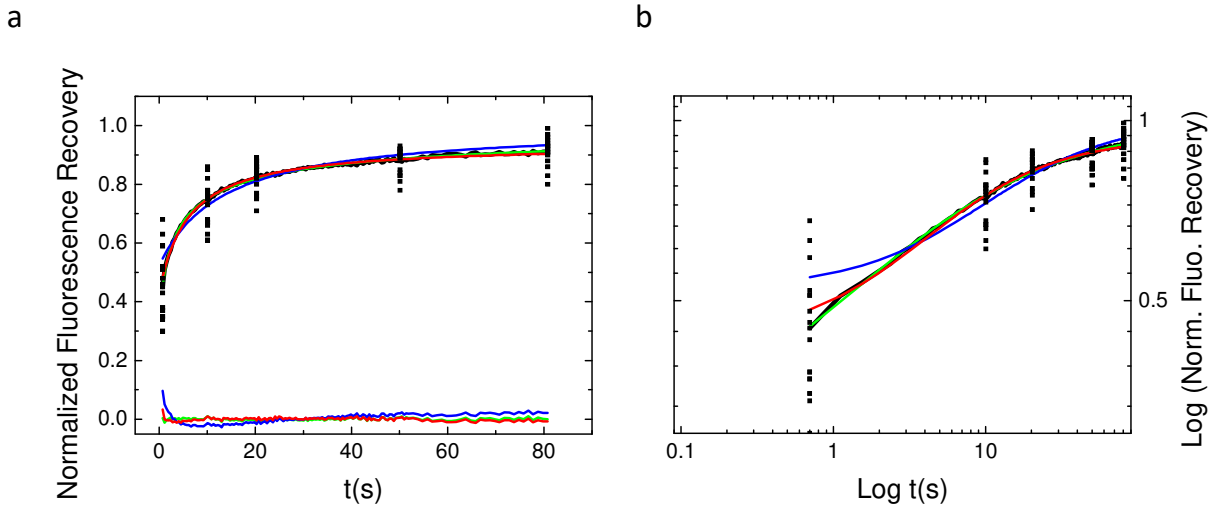

Figure 3. Average experimental recovery curve fitted by the three diffusion models. The three models (bM, rBm and aDm) were used to fit the average recovery curve obtained from 45 different experiments. The normal (part **a**) plot shows the residual from the fit of the different models. Note that only the bM model fit is inaccurate. The Log-Log plot (part **b**) illustrate again the difficulty to discriminate between the aDm and the rBm model in the goodness of the fit.

Figure3 shows the average fluorescence recovery (black line, mean of the 45 recoveries) as well as some points extracted from of the 45 different recoveries in order to illustrate the discrepancy observed when working with cells. This mean fluorescence recovery has been fitted by the three different models used in the previous section. On the bottom of Fig. 3a is depicted the differences between the fit and the observed fluorescence ($F_f - F_o$) in order to illustrate the quality of the fit. From figure 3a (normal plot) and figure 3b (log-log plot) it can easily be seen that except for the free Brownian motion model(Bm), the nature of the diffusion of PH-EFA6 cannot be discriminated between restricted Brownian motion (rBm) and anomalous diffusion (aDm). This is confirmed by a χ^2 statistical test to probe the quality of the fit as shown in table 1. Table 1 also summarized the average values of the set of parameters (D, M, D_α, α) that can be extracted from the different fits.

Table 1. Parameters values obtained by the fit of the average experimental recovery with the different analytical models

Model	$D(\mu m.s^{-1})$	**M**	α	$D_\alpha(\mu m.s^{-\alpha})$	χ^2
Bm	0.12±0.06	1	-	-	5.7±0.5
rBm	0.22±0.01	0.92±0.01	-	-	3.8±1.6
aDm	-	-	0.65±0.02	1.48±0.05	2.9±1.6

2.5. Variable radii FRAP allows correct estimation of the anomalous sub-diffusion exponent α

Previous results using direct analysis on both numerically simulated recoveries and experimental recoveries clearly showed that : i) Parameters α and D_α) of the aDm model were always underestimated ii) aDm and rBm models could only be discriminated at short and long times. Nevertheless, since time and space are correlated in diffusion and since experimental time-scale is finite, variable radii FRAP experiments were firstly numerically simulated and performed after on cells (see experimental section

Preprints (www.preprints.org) | NOT PEER-REVIEWED | Posted: 19 July 2018 doi:10.20944/preprints201807.0356.v1

Peer-reviewed version available at Biomolecules 2018, 8, 90; doi:10.3390/biom8030090

for explanation). Each parameter (α and D_α) were estimated again, by fitting simulated recoveries at different radius (see Monte-Carlo simulation section for explanation) with our analytical model (eq. 8). Figure 4 shows the behaviour of fitted a as a function of 1/R. Theory of anomalous diffusion processes predicts that a is space-invariant in a "homogeneously heterogeneous" environment. It can be directly seen on the plot that this is not what our data suggest, but on the opposite they showed that a linear dependence of α as a function of 1/R (at least for R > 1 a.u.) with a negative slope is observed for the

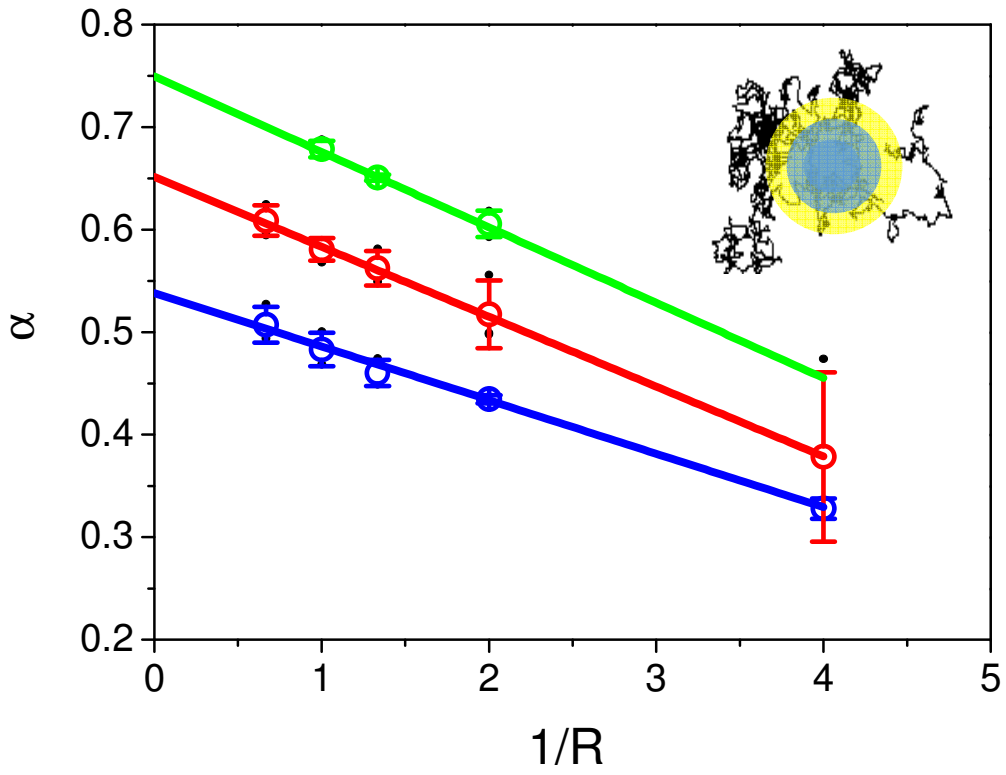

Figure 4. Values of α obtained from the fit of CTRW simulated recoveries as a function of $1/R$. Values of α introduced in the fit were respectively 0.6 (in blue), 0.7 (in red), 0.8 (in green). Dots represent the mean $\pm$ s.d. values of α obtained with the fit using eq. 8 of simulated recoveries for a set of D values (0.01, 0.05, 0.1, 0.5, 1, 2, 3, black dots in the graph). Extrapolation at $1/R = 0$ of the linear fit of the different $alpha$ obtained from the fits of recoveries at different radius gives $alpha$ values close to the one used for the simulations.

Similar results were obtained when plotting D fitted as a function of 1/R . Therefore, in order to test the hypothesis that α and D could be correctly determined by performing linear regressions of fitted values of both parameters as a function of 1/R, a set of numerical simulation were performed using different D, α and R. Values of α and D at $1/R = 0$ intercepts are resumed in Appendix fig. A2. Fig.A2a and A2b show that, except for few values, when using this approach, α and D can be estimated with an error of less than 5 % of their real values. With regards to the discrepancy of the experiments on cells, this uncertainty seems enough accurate for correct determination of both parameters in case of anomalous diffusion processes using variable radii.

Preprints (www.preprints.org) | NOT PEER-REVIEWED | Posted: 19 July 2018 doi:10.20944/preprints201807.0356.v1

Peer-reviewed version available at Biomolecules 2018, 8, 90; doi:10.3390/biom8030090

2.6. CTRW anomalous subdiffusion does not explain PH-EFA6 motions at the plasma membrane of BHK cells.

Variable radii FRAP has already been proposed by Salomé et al. in order to characterize membrane domains in cells [5]. They found both by numerical simulation and by experimental approaches that fitting recovery curves using the rBm model lead to a linear regression of the mobile fraction (M) as a function of 1/R with a positive slope. In this study our results show that the same approach is valid with aDm model and that plotting of a as a function of 1/R led to a linear regression with a negative slope. Therefore several experiments (n<30) has been performed on cells expressing the PH domain of EFA6 at variable radii of photodestruction. Experimental recoveries were fitted with both models (aDm and fBm).

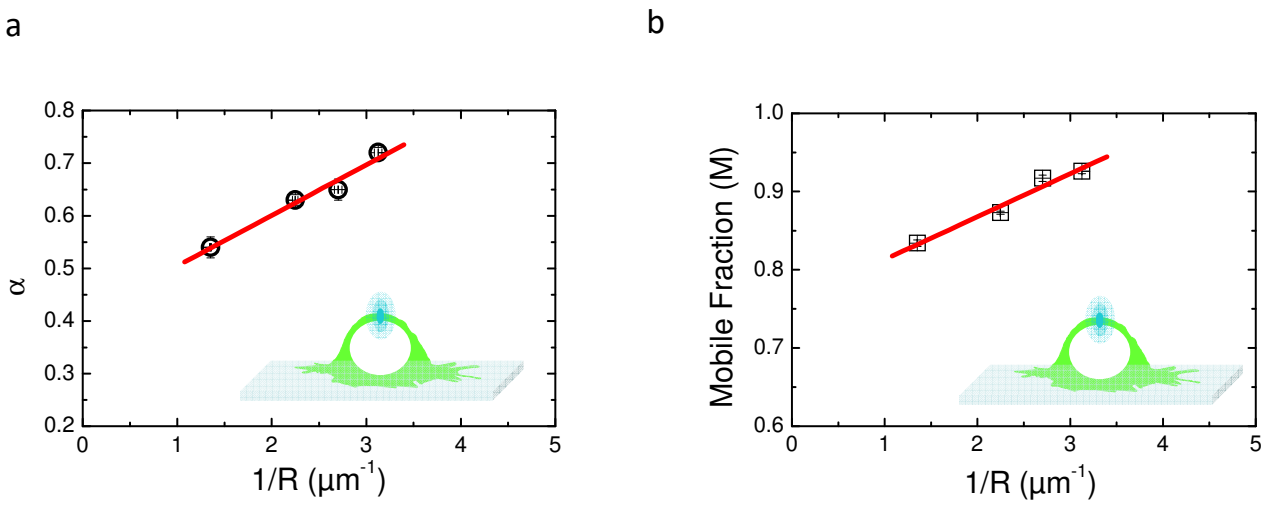

Figure 5. Comparison of the two models aDm and rBm using vrFRAP in the case of PH-EFA6 diffusion at the plasma membrane of BHK cells a: Plot of α values obtained by fitting the experimental recoveries with eq. 8 as a function of 1/R. The plot exhibit a positive slot in opposite to the one observed in Fig. 4, suggesting an absence of a CTRW anomalous sub-diffusion in the motion of PH-EFA6. **b**: Plot of M value obtained by fitting the experimental recoveries with eq. 10 as a function of 1/R. The plot exhibit a positive slope as obsreved in [25] and [5], suggesting a diffusion with trapping in spatial domains.

Figure 5 shows the behaviour of the characteristic parameters of each model (α for aDM and M for rBm) as a function of 1/R. In Fig.5a is depicted the linear dependence of experimental α as a function of 1/R. This results clearly show a positive slope for the regression, suggesting that the aDm model is not the correct model for the analysis of diffusion in the case of PH-EFA6 in this experimental time and length scale. On the opposite, Fig.5b, where M is plotted as a function of 1/R clearly shows a positive slope as already observed in Salomé's work [5]. This shows that, in the case of PH-EFA6 diffusion at the plasma membrane of BHK cells, the rBm is the more appropriate model to describe the restriction of diffusion observed in FRAP experiments.

Preprints (www.preprints.org) | NOT PEER-REVIEWED | Posted: 19 July 2018 doi:10.20944/preprints201807.0356.v1

Peer-reviewed version available at Biomolecules 2018, 8, 90; doi:10.3390/biom8030090

Schram *et al.* empiricaly determined a relationship between the size of the trapping domains (L) and the variation of the mobile fraction (M) [25] :

$$M = M_p + \frac{0.63.L}{R}; L < R \tag{11}$$

Using eq.11, we could determine that 75% of PH-EFA6 molecules exhibit free diffusion while the 25 % left are confined in domains of approximately 90 nm radius.

3. Discussion

This work has been initiated to characterize the nature of the diffusion of molecules binding the inner leaflet of the cell plasma membranes by means of FRAP experiments. In a first attempt, we decided to compare experimental data obtained with the PH domain of EFA6 expressed in BHK cells to FRAP curves generated from anomalous sub-diffusive particles numerically simulated. Then, we analyzed the recoveries with three different diffusion models, namely the pure Brownian motion (Bm), the restricted Brownian motion (rBm) and the CTRW anomalous subdiffusion (aDm). Four parameters can be extracted from these diffusion models. The Brownian diffusion coefficient D and the mobile fraction M (M=1 in the case of Bm) on one side, and the anomalous subdiffusion exponent α and its related anomalous diffusion coefficent D_α on the other side. The aDm model has been extensively studied by numerical simulations. Direct analysis of numerically simulated curves lead to an underestimation of D_α and α. This was already observed by Feder *et al.* whom proposed, in order to circumvent this underestimation, to add a mobile fraction (M) as a new parameter [15]. On a physical point of view this is incorrect since the phenomenological parameter "mobile fraction" is indeed a part of α as discussed by Nagle *et al.* [24]. This underestimation of D_α and α is mainly due to finite size effect (space and time) that cannot be easily overcome neither in simulations nor in experiments. We directly tested for anomalous sub-diffusion in the simulated and experimental curves by fitting the recovery curves with normal and anomalous equations and look for systematic deviations of the fit, both in linear plots to see the fit at large times and log-log plots to see the fit at short times. From this approach we could see that the Bm can be immediately discarded. The difference between the aDm and the fBm could only be observed at very short times (log-log plots) and very long times. Unfortunately, these two extrema times are hardly easy to analyse in experiments. Indeed, at short times the curve may be distorted by diffusion during the bleach pulse [26] and limits in the frequency of data collection. At long times, motion of the membrane or photobleaching of the fluorescent probe might appear. This is illustrated here in our experimental data. Fits of single spot fluorescence recoveries did not allow to determine without uncertainties which of the aDm or the rBm model reflect the nature of PH-EFA6 diffusion at the plasma membrane of BHK cells. Although underestimated, the α value we found here, when fitting with the aDm model, reflect a strong deviation from the Brownian motion and suggest that PH-EFA6 explores a strongly compartmentalized landscape while travelling at the inner leaflet of the plasma membrane. Nevertheless, this α value, as well as the M value in the case of the rBm model are higher than the one found for IgE receptor transmembrane protein in RBL cells ($\alpha = 0.46 \pm 0.22$) [15]. Using single particle tracking experiments, other transmembrane proteins such as MHC class I in HeLa cells has also been shown to exhibit anomalous subdiffusion with an α value close to 0.5 [27]. On the opposite, other transmembrane proteins exhibit high α values (α=0.8) (Kv2.1 potassium channel in HEK293T cells [28]) or pure Brownian motion (MHC class II in CHO cells [29] or aquaporin-1 in MDCK cells [30].

The inability of FRAP to cover several time decades as SPT or FCS techniques can be overcome by probing the environment at different space scale using variable radii FRAP [5,6]. Here we have simulated recoveries in the case of CTRW anomalous subdiffusion at different space scales and fit them with the aDm model in order to extract the set of parameters (α, D). By monitoring the change of fitted (α, D) parameters as a function of space (1/R) we observed that the fitted values of α decreased with decreasing radius of observation. We showed that the correct values of α and D could be determined

Preprints (www.preprints.org) | NOT PEER-REVIEWED | Posted: 19 July 2018 doi:10.20944/preprints201807.0356.v1

Peer-reviewed version available at Biomolecules 2018, 8, 90; doi:10.3390/biom8030090

at $1/R = 0$, i.e. when $R \to \infty$. This is one way to overcome the finite size effect of the measurements. Then, we apply this approach to the experimental recoveries obtained at different radii. Surprisingly we observed the opposite tendency to the one observed in our simulation, suggesting that the CTRW anomalous subdiffusion is not the correct model to describe the motion of PH-EFA6 in BHK cells. On the opposite, when monitoring the change of the mobile fraction obtained by fitting the experimental recoveries with the rBm model, we observed the same tendency as the one described in [5] and [31], i.e., an increase of the mobile fraction with a decreasing radius. Using this approach, we could determine that 25% of PH-EFA6 molecules are confined in domains of 90 nm radius.

CTRW is not the only source of anomalous sub-diffusion. The experimental increase of α with decreasing radius can also be an apparent consequence of a cross over regime with two different diffusion coefficient as it is described by the rBm model in this study. Using FCS experiments and simulations at different radii of a two phases two component lipid mixtures at different temperature, Favard *et al.* showed that changes in anomalous sub-diffusion exponent α could nicely predict the phase transitions temperatures but failed in determining the average size of domains coexisting in the two-phases [2]. On the opposite by monitoring the change in diffusion regimes, they could nicely determine the mean size of the gel-phase domains. If we extend this approach to our $alpha$ plot as a function of the probes radius, we see that the transition from anomalous sub-diffusion ($\alpha < 1$) to normal diffusion ($\alpha = 1$) occurs at radius of 160 nm, i.e., not far from the values obtained with the rBm model.

The range of domain sizes observed here (90 to 160 nm radius), independently of the model used to describe the dynamics of PH-EFA6, is likely to be due to subcortical actin cytoskeleton. Equivalent sizes has been observed in NRK cells [32] using electron microscopy, and recently in several cell lines, by monitoring membrane lipids dynamics using STED-FCS [33]. Interestingly, Krapf *et al.* described that this meshwork has a fractal dimension and could therefore lead to anomalous sub-diffusion [34]. Therefore, further investigations and numerical simulations using a meshwork with fractal dimension as the origin of the anomalous sub-diffusion are likely to be conducted in order to understand the origin of our $\alpha = f(1/R)$ behaviour in our vrFRAP experiments.

In conclusion, by performing FRAP at variable radii, we found a way to discriminate CTRW induces anomalous sub-diffusion from other restricted motion at the plasma membrane of living cells. We also show that, while travelling at the inner leaflet of the plasma membrane, PH-EFA6 is not stopped in various traps with different residence times but on the opposite is mainly freely diffusing with on average 25% of the molecules confined in 90-160 nm radius open domains most probably due to the actin cortical cytoskeleton.

4. Materials and Methods

4.1. Monte Carlo Simulation

In order to keep in our calculation the finite size effects, the simulation were made in a ring of a radius of 30 arbitrary unit (a.u.) length explored by 106 particles for each run. Radii varying from 0.5 to 3 a.u. were photo-destructed. Reflective type of boundary conditions were used. This means that when a particle gets out of the 30 a.u. radius it is re-introduced in the same direction at a small distance of the boundary.

4.2. Cell culture and transfection

Baby hamster kidney cells (BHK) were grown on a coverslip in BHK-21 medium (Gibco-BRL), containing 5% FCS, 10% Tryptose phosphate broth, 100U/ml penicillin, 100 μg/ml stretomycin and 2mM L-Glutamine. Cells were transfected using Fugene 36 hours before the FRAP experiments with a pC1EGFPPHEFA6 plasmid. Fugene containing medium was replaced 12 h before the experiments by fresh medium. pC1EGFPPHEFA6 contains the sequence for both PH-EFA6 domain and EGFP as a

Preprints (www.preprints.org) | NOT PEER-REVIEWED | Posted: 19 July 2018 doi:10.20944/preprints201807.0356.v1

Peer-reviewed version available at Biomolecules 2018, 8, 90; doi:10.3390/biom8030090

fluorescent label, linked to the N-terminus of the PH-EFA6 domain in order to avoid any perturbation to the membrane linkage.

4.3. FRAP experiments

FRAP measurements were made with a commercially available confocal microscope, Leica TCS-SP1 (Leica Microsystems, Germany). Prebleached images were firstly acquired to ensure for the lack of photo-destruction during the observation. A brief laser pulse (200 ms) was then delivered to the cell on a given and fixed position. Images were thereafter recorded at given intervals (440 ms) using a spectral window for fluorescence emission between 500 and 600 nm. The intensity ratio between the extinction laser beam and the monitoring laser beam was fixed to 10^6. Each fluorescence recovery was recorded for 100 s at 25○C, containing 150 experimental values (Recovery curve was sampled every 0.44 s in the beginning and 1 s in the end to avoid photobleaching during the monitoring). Focusing the laser by the microscope objectives produced a Gaussian intensity distribution of the beam in the object plane. This distribution was monitored using NBD-PC labelled DPPC multilamellar preparation at 25○C (T<Tm). Since no diffusion occurs at this temperature, the image obtained immediately after the end of the bleaching pulse shows a "hole" in the fluorescent preparation that allow measurement of the laser waist and determination of the intensity profile in the x,y plane. These measurements were confirmed by the use of fluorescent beads with a maximum wavelength of emission at 500 nm [35]. The following values were obtained for the waist as a function of the objective used :

Table 2. Size of the different radius measured with the objectives used in this work.

Objective	R (μm)	ΔR (μm)	laser waist (nm)
16x (NA=1.0)	0.74	0.04	370
40x (NA=1.3)	0.44	0.03	222
63x (NA=1.4)	0.37	0.01	185
100x(NA=1.4)	0.32	0.01	160

Funding: 'This research received no external funding"

Acknowledgments: Author would like to acknowledge M. Franco for the gift of the PH-EFA6 plamsid and discussion. I am indebted to JL Meunier for the numerical simulations of the FRAP recoveries. The author also thank A. Lopez and N. Olivi-Tran for fruitful discussions. THe author is a member of the IMABIO CNRS consortium. Most of this work has been realized during the author stay at the IPMC CNRS UMR 7275.

Conflicts of Interest: "The authors declare no conflict of interest."

Abbreviations

The following abbreviations are used in this manuscript:

FRAP	Fluorescence Recovery After Photobleaching
vrFRAP	variable radii Fluorescence Recovery After Photobleaching
FCS	Fluorescence Coreelation Spectroscopy
SPT	Single Particle Tracking
CTRW	Continuous-Time Random Walk
aDm	anomalous subdiffusion motion
Bm	Brownian motion
rBm	restricted Brownian motion
PH-EFA6	Pleckstrin Homology domain of Exchange Factor for ARF-6

Preprints (www.preprints.org) | NOT PEER-REVIEWED | Posted: 19 July 2018 doi:10.20944/preprints201807.0356.v1

Peer-reviewed version available at Biomolecules 2018, 8, 90; doi:10.3390/biom8030090

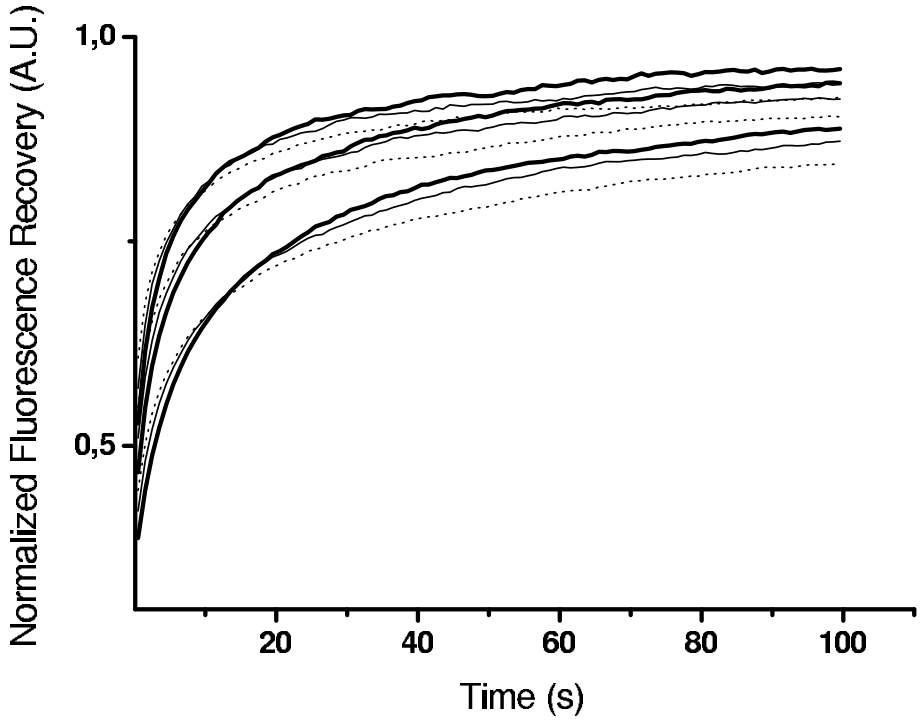

Figure A1. Monte-Carlo simulation of normalized fluorescence recoveries in the case of CTRW anomalous subdiffusion . Different values of D and α have been tested in the simulations. Here, values of $D = 0.5; 1; 1.5$ are represented from bottom to top with different α in each case : 0.6 (dots) ; 0.7 (thin line) ; 0.8 (thick line). The Monte Carlo has been constructed with 10^7 individual trajectories

Appendix A. Examples of Numerical Generated Fluorescence Recovery Curves

Figure A1 depicts some fluorescence recovery curves obtained with our numerical simulations for different D and α inserted in the simulation.

Preprints (www.preprints.org) | NOT PEER-REVIEWED | Posted: 19 July 2018 doi:10.20944/preprints201807.0356.v1

Peer-reviewed version available at Biomolecules 2018, 8, 90; doi:10.3390/biom8030090

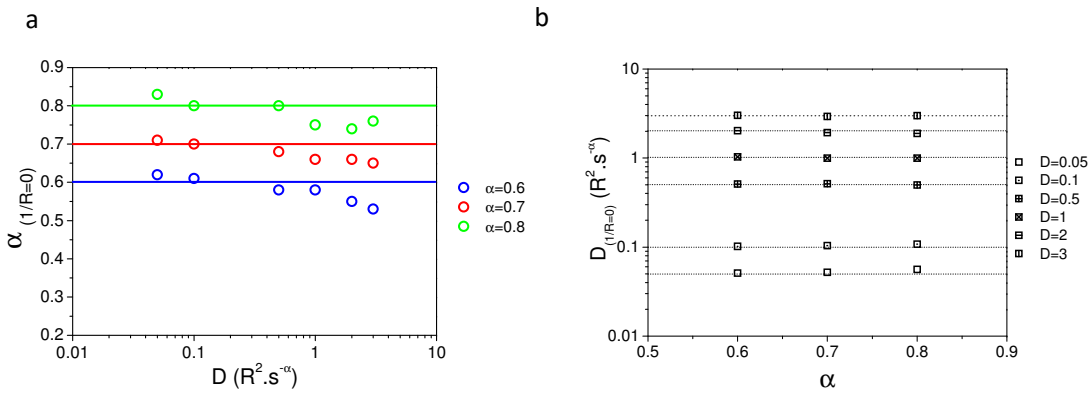

Figure A2. Values of α (fig. A2 a) and D (fig. A2 b) at $1/R = 0$ intercepts.

Appendix B. Comparison of input and fitted D and α at variable radii

In figure A2 are plotted values of α (fig. A2 a) and D (fig. A2 b) at $1/R = 0$ intercepts. Fig.A2a and A2b show that extrapolated $\alpha_{(1/R=0)}$ and extrapolated $D_{(1/R=0)}$ are found to be with an error of less than 5 % of their simulation inserted values.

References

1. Singer, S.J.; Nicolson, G.L. The Fluid Mosaic Model of the Structure of Cell Membranes. *Science* **1972**, *175*, 720–731. doi:10.1126/science.175.4023.720.
2. Favard, C.; Wenger, J.; Lenne, P.F.; Rigneault, H. FCS diffusion laws in two-phase lipid membranes: determination of domain mean size by experiments and Monte Carlo simulations. *Biophysical journal* **2011**, *100*, 1242–1251. doi:10.1016/j.bpj.2010.12.3738.
3. Hac, A.E.; Seeger, H.M.; Fidorra, M.; Heimburg, T. Diffusion in two-component lipid membranes–a fluorescence correlation spectroscopy and monte carlo simulation study. *Biophys. J.* **2005**, *88*, 317–333. doi:10.1529/biophysj.104.040444.
4. Edidin, M.; Kuo, S.C.; Sheetz, M.P. Lateral movements of membrane glycoproteins restricted by dynamic cytoplasmic barriers. *Science* **1991**, *254*, 1379–1382. doi:10.1126/science.1835798.
5. Salomé, L.; Cazeils, J.L.; Lopez, A.; Tocanne, J.F. Characterization of membrane domains by frap experiments at variable observation areas. *Eur Biophys J* **1998**, *27*, 391–402. doi:10.1007/s002490050146.
6. Yechiel, E.; Edidin, M. Micrometer-scale domains in fibroblast plasma membranes. *The Journal of Cell Biology* **1987**, *105*, 755–760. doi:10.1083/jcb.105.2.755.
7. Lingwood, D.; Simons, K. Lipid rafts as a membrane-organizing principle. *Science* **2010**, *327*, 46–50. doi:10.1126/science.1174621.
8. Kusumi, A.; Sako, Y.; Yamamoto, M. Confined lateral diffusion of membrane receptors as studied by single particle tracking (nanovid microscopy). Effects of calcium-induced differentiation in cultured epithelial cells. *Biophysical Journal* **1993**, *65*, 2021–2040. doi:10.1016/S0006-3495(93)81253-0.
9. Sako, Y.; Kusumi, A. Compartmentalized structure of the plasma membrane for receptor movements as revealed by a nanometer-level motion analysis. *J. Cell Biol.* **1994**, *125*, 1251–1264.
10. Wawrezinieck, L.; Rigneault, H.; Marguet, D.; Lenne, P.F. Fluorescence correlation spectroscopy diffusion laws to probe the submicron cell membrane organization. *Biophys. J.* **2005**, *89*, 4029–4042. doi:10.1529/biophysj.105.067959.
11. Lenne, P.F.; Wawrezinieck, L.; Conchonaud, F.; Wurtz, O.; Boned, A.; Guo, X.J.; Rigneault, H.; He, H.T.; Marguet, D. Dynamic molecular confinement in the plasma membrane by microdomains and the cytoskeleton meshwork. *EMBO J.* **2006**, *25*, 3245–3256. doi:10.1038/sj.emboj.7601214.
12. Eggeling, C.; Ringemann, C.; Medda, R.; Schwarzmann, G.; Sandhoff, K.; Polyakova, S.; Belov, V.N.; Hein, B.; von Middendorff, C.; Schönle, A.; Hell, S.W. Direct observation of the nanoscale dynamics of membrane lipids in a living cell. *Nature* **2009**, *457*, 1159–1162. doi:10.1038/nature07596.
13. Axelrod, D.; Koppel, D.E.; Schlessinger, J.; Elson, E.; Webb, W.W. Mobility measurement by analysis of fluorescence photobleaching recovery kinetics. *Biophysical Journal* **1976**, *16*, 1055–1069. doi:10.1016/S0006-3495(76)85755-4.
14. Soumpasis, D.M. Theoretical analysis of fluorescence photobleaching recovery experiments. *Biophysical Journal* **1983**, *41*, 95–97. doi:10.1016/S0006-3495(83)84410-5.
15. Feder, T.J.; Brust-Mascher, I.; Slattery, J.P.; Baird, B.; Webb, W.W. Constrained diffusion or immobile fraction on cell surfaces: a new interpretation. *Biophysical Journal* **1996**, *70*, 2767–2773. doi:10.1016/S0006-3495(96)79846-6.
16. Bouchaud, J.P.; Georges, A. Anomalous diffusion in disordered media: Statistical mechanisms, models and physical applications. *Physics Reports* **1990**, *195*, 127–293. doi:10.1016/0370-1573(90)90099-N.
17. Hoefling, F.; Franosch, T. Anomalous transport in the crowded world of biological cells. *Rep. Prog. Phys.* **2013**, *76*, 046602. WOS:000317032800007, doi:10.1088/0034-4885/76/4/046602.
18. Saxton, M.J. Anomalous diffusion due to obstacles: a Monte Carlo study. *Biophysical Journal* **1994**, *66*, 394–401. doi:10.1016/S0006-3495(94)80789-1.
19. Saxton, M.J. Anomalous diffusion due to binding: a Monte Carlo study. *Biophysical Journal* **1996**, *70*, 1250–1262. doi:10.1016/S0006-3495(96)79682-0.
20. Saxton, M.J. Anomalous Subdiffusion in Fluorescence Photobleaching Recovery: A Monte Carlo Study. *Biophysical Journal* **2001**, *81*, 2226–2240. doi:10.1016/S0006-3495(01)75870-5.
21. Hyvönen, M.; Macias, M.J.; Nilges, M.; Oschkinat, H.; Saraste, M.; Wilmanns, M. Structure of the binding site for inositol phosphates in a PH domain. *The EMBO Journal*, *14*, 4676–4685. doi:10.1002/j.1460-2075.1995.tb00149.x.

22. Franco, M.; Peters, P.J.; Boretto, J.; Donselaar, E.v.; Neri, A.; D'Souza-Schorey, C.; Chavrier, P. EFA6, a sec7 domain-containing exchange factor for ARF6, coordinates membrane recycling and actin cytoskeleton organization. *The EMBO Journal* **1999**, *18*, 1480–1491. doi:10.1093/emboj/18.6.1480.
23. Macia, E.; Partisani, M.; Favard, C.; Mortier, E.; Zimmermann, P.; Carlier, M.F.; Gounon, P.; Luton, F.; Franco, M. The pleckstrin homology domain of the Arf6-specific exchange factor EFA6 localizes to the plasma membrane by interacting with phosphatidylinositol 4,5-bisphosphate and F-actin. *The Journal of biological chemistry* **2008**, *283*, 19836–19844. doi:10.1074/jbc.M800781200.
24. Nagle, J.F. Long tail kinetics in biophysics? *Biophysical Journal* **1992**, *63*, 366–370. doi:10.1016/S0006-3495(92)81602-8.
25. Schram, V.; Tocanne, J.F.; Lopez, A. Influence of obstacles on lipid lateral diffusion: computer simulation of FRAP experiments and application to proteoliposomes and biomembranes. *Eur Biophys J* **1994**, *23*, 337–348. doi:10.1007/BF00188657.
26. Waharte, F.; Brown, C.M.; Coscoy, S.; Coudrier, E.; Amblard, F. A two-photon FRAP analysis of the cytoskeleton dynamics in the microvilli of intestinal cells. *Biophys. J.* **2005**, *88*, 1467–1478. doi:10.1529/biophysj.104.049619.
27. Smith, P.R.; Morrison, I.E.; Wilson, K.M.; Fernández, N.; Cherry, R.J. Anomalous diffusion of major histocompatibility complex class I molecules on HeLa cells determined by single particle tracking. *Biophys. J.* **1999**, *76*, 3331–3344. doi:10.1016/S0006-3495(99)77486-2.
28. Weigel, A.V.; Simon, B.; Tamkun, M.M.; Krapf, D. Ergodic and nonergodic processes coexist in the plasma membrane as observed by single-molecule tracking. *Proc. Natl. Acad. Sci. U.S.A.* **2011**, *108*, 6438–6443. doi:10.1073/pnas.1016325108.
29. Vrljic, M.; Nishimura, S.Y.; Brasselet, S.; Moerner, W.E.; McConnell, H.M. Translational diffusion of individual class II MHC membrane proteins in cells. *Biophys. J.* **2002**, *83*, 2681–2692. doi:10.1016/S0006-3495(02)75277-6.
30. Crane, J.M.; Verkman, A.S. Long-range nonanomalous diffusion of quantum dot-labeled aquaporin-1 water channels in the cell plasma membrane. *Biophys. J.* **2008**, *94*, 702–713. doi:10.1529/biophysj.107.115121.
31. Baker, A.M.; Saulière, A.; Gaibelet, G.; Lagane, B.; Mazères, S.; Fourage, M.; Bachelerie, F.; Salomé, L.; Lopez, A.; Dumas, F. CD4 interacts constitutively with multiple CCR5 at the plasma membrane of living cells. A fluorescence recovery after photobleaching at variable radii approach. *J. Biol. Chem.* **2007**, *282*, 35163–35168. doi:10.1074/jbc.M705617200.
32. Morone, N.; Fujiwara, T.; Murase, K.; Kasai, R.S.; Ike, H.; Yuasa, S.; Usukura, J.; Kusumi, A. Three-dimensional reconstruction of the membrane skeleton at the plasma membrane interface by electron tomography. *J. Cell Biol.* **2006**, *174*, 851–862. doi:10.1083/jcb.200606007.
33. Andrade, D.M.; Clausen, M.P.; Keller, J.; Mueller, V.; Wu, C.; Bear, J.E.; Hell, S.W.; Lagerholm, B.C.; Eggeling, C. Cortical actin networks induce spatio-temporal confinement of phospholipids in the plasma membrane – a minimally invasive investigation by STED-FCS. *Scientific Reports* **2015**, *5*, 11454. doi:10.1038/srep11454.
34. Sadegh, S.; Higgins, J.L.; Mannion, P.C.; Tamkun, M.M.; Krapf, D. Plasma Membrane is Compartmentalized by a Self-Similar Cortical Actin Meshwork. *Phys. Rev. X* **2017**, *7*, 011031. doi:10.1103/PhysRevX.7.011031.
35. Schneider, M.B.; Webb, W.W. Measurement of submicron laser beam radii. *Appl Opt* **1981**, *20*, 1382–1388.